JET-P(96)34

Analysis of Fast Minority Ion Distribution and Current Generation for ICRF and LH Heating

J A Heikkinen[1], T P Kiviniemi[2], M J Mantsinen[2], A Saveliev[3], L-G Eriksson, T J H Pättikangas[1], S K Sipilä[2], A Piliya[3].

JET Joint Undertaking, Abingdon, Oxfordshire, OX14 3EA, UK.
[1] VTT Energy, Association EURATOM-TEKES, PO Box 1604, FIN-02044, VTT, Finland.
[2] Helsinki University of Technology, Department of Technical Physics, FIN-02150 Espoo, Finland.
[3] A F Ioffe Physico-Technical Institute, St Petersberg 194021, Russia.

Preprint of a paper to be submitted for publication in
Plasma Physics and Controlled Fusion

September 1996

ABSTRACT

Dynamics of fast minority ions energised by ion cyclotron resonance and lower hybrid heating in tokamaks is investigated by cylindrical 2D Fokker-Planck and toroidal 3D Monte Carlo calculations. The power exchange between the waves and minority ions, the ensuing fast ion bootstrap current and the power deposition are calculated in the presence of fast ion radial diffusion and thermal minority ion source near the plasma edge. Both lower hybrid and ion cyclotron heating are observed to increase by increasing overlapping of the heating regimes and by radial diffusion, because of the enhanced diffusion of the ion cyclotron heated ions from their resonance region to the peripheral lower hybrid wave region, and diffusion of thermal ions from the plasma edge to the ion cyclotron heating region. The fast minority ion current is found to be strongly modified by the bootstrap current generation in the cyclotron heating region. An analytical expression to describe the RF-induced bootstrap current is presented.

1. INTRODUCTION

During recent years, the interaction of energetic ions with radiofrequency (RF) waves has attracted much interest because of the importance of the interaction of the transport and heating of plasma ions or charged fusion products like alpha particles or protons in RF-heated tokamak reactors. The absorption of fast magnetosonic waves and lower hybrid (LH) waves by, for example, alpha particles [1,2] has been investigated in a great detail for tokamak configuration. Also, the absorption of LH waves by minority ions produced in ion cyclotron resonance (ICRF) heating has been evaluated [3]. Although many of these works have treated the wave propagation and power deposition in a relatively detailed way, only very few studies have considered whether the radial diffusion of the heated ions affects the power absorption and whether the heating can generate currents. The effects of finite ion orbits on the wave-driven ICRF minority current [4,5] and on the minority bootstrap current [6] have been investigated only very recently. It has been also suggested [7] that, under certain conditions, the free expansion energy related to the wave-induced radial diffusion in the wave-alpha interaction could alter the direction of power transfer between the wave and alpha particles.

In recent fully toroidal Monte Carlo simulation [8] of the interaction of isotropically produced fusion alpha population from deuterium-tritium (DT) reactions with off-axis localised lower hybrid waves, reduction of the alpha absorption of the LH wave power by the wave induced radial alpha diffusion and a strong enhancement of the alpha bootstrap current with a formation of a bipolar current density profile were observed. Similar interaction as for alpha particles can also be envisaged for the ICRF-produced fast minority ions which can attain comparable or even higher particle energy and concentration than alpha particles. The local heating of minority ions around the cyclotron resonance acts as a strong source of diamagnetic

current with local off-axis modification of the safety factor and shear which can be attractive for plasma stabilisation and confinement improvement. Here, the necessary control of the position of current profile modification is easier for the ICRF interaction than for the LH interaction. On the other hand, if the ICRF heating and LH heating regimes would overlap, synergistic effects might be possible. It is therefore of interest to study the diffusion and distribution of ICRF heated minority ions, created ion current, and the interaction of the ions with an off-axis lower hybrid wave field structure for which the balance [9] of wave absorption and wave penetration in a torus determines the position relative to the cyclotron heating domain. It is important to evaluate the profiles of power deposition, fast ion current, and concentration in the absence and presence of radial diffusion. The latter diffusion can originate from various mechanisms like the magnetic ripple or instabilities, which determine the recycling of thermal minority ions and ICRF heated ions between the plasma edge and the plasma core.

The calculations of the previous quantities by Monte Carlo guiding centre code simulations and by a two-dimensional Fokker-Planck code are presented in this work. Main results are shown for an axisymmetric tokamak with circular cross-section and with prescribed radial profiles of the ICRF diffusion operators and with the LH diffusion coefficient obtained from ray-tracing. A model for the fast ion bootstrap current calculation is presented which makes the fast estimate of the current possible with reduced-order Fokker-Planck solutions of the ion distribution in velocity and configuration space. Comparison with the fully toroidal Monte Carlo simulation results are presented. Recently, Ramos de Andrade *et al.* [3] evaluated the LH wave absorption on the ICRF-produced minority ions based on simplified one-dimensional Fokker-Planck solutions for the velocity distribution, and obtained up to 25% absorption of the LH power by fast ions under specific JET plasma conditions. In the present work, the effects from the full toroidal model and radial dependence are considered and their importance with respect to the previous calculations are assessed.

In Section 2, the model used to describe the fast ion production by ICRF heating, the ion interaction with the LH wave, and the ensuing fast ion bootstrap current are presented. The two-dimensional Fokker-Planck and the toroidal guiding-centre code for solving the ion velocity distribution, ion heating, and the produced ion current are shortly discussed.

Section 3 describes the results which have been obtained with the adopted models. Discussion of the results is given in Section 4.

2. MODELLING OF MINORITY ION INTERACTION WITH LH AND ICRF WAVES.

2.1 Analytical Model

Our analysis is based on the drift equation [10] for the minority ion distribution function $f(t,\varphi,\theta,v_\perp,v_\parallel)$ in an axisymmetric tokamak with a circular cross-section

$$\frac{\partial f}{\partial t}+v_\parallel\frac{B_\theta}{rB}\left[\frac{\partial f}{\partial\theta}+\frac{I}{\Omega_0}\frac{\partial f}{\partial\varphi}\frac{\partial}{\partial\theta}(v_\parallel h)\right]=C(f)+Q_{LH}(f)+Q_{IC}(f)+S(f,v). \qquad (1)$$

Here, C(f) is the Fokker-Planck collision operator, and S(f,v) stands for the non-RF operators describing, for example, any anomalous radial diffusion of the ions or their source. The distribution function is given as a function of time t, the poloidal flux function $\varphi=\int^r B_\theta R dr$, the poloidal angle θ, and the particle velocity components $v_\parallel$ and $v_\perp$. The velocity components $v_\parallel=\pm v\sqrt{1-\lambda/h}$ and $v_\perp$ refer to the parallel and perpendicular direction, respectively, with respect to the magnetic field $\vec{B}=I\nabla\phi+\nabla\phi\times\nabla\varphi$, where ϕ is the toroidal angle. The radius of the flux surface φ is r, the poloidal magnetic field component is $B_\theta,\lambda=v_\perp^2 h/v^2, h\equiv B_0/B=1+\varepsilon\cos\theta$, $\varepsilon=r/R_0$ is the inverse aspect ratio and the subindex 0 denotes the value at the magnetic axis r = 0. The toroidal flux function $I(\varphi)$ is given approximately with I = BR, where $R = R_0 h$ is the local major radius. $\Omega = qB/m$ is the gyrofrequency of the minority ion, and q and m are the charge and mass of the ion.

We have introduced the lower hybrid wave operator [11]

$$Q_{LH}=\frac{1}{s}Ls\frac{D_{LH}}{\sqrt{v_\perp^2-\omega_L^2/k_{L\perp}^2}}Lf \qquad (2)$$

with

$$L=\frac{1}{v_\perp}\frac{\partial}{\partial v_\perp}+G_v\frac{\partial}{\partial v_\parallel}+G_r\frac{\partial}{\partial r}, \qquad (3)$$

$G_v=(k_\parallel/\omega_L)\beta$, $G_r=(k_\eta/\omega_L\Omega)\beta$, and $\beta=(1-k_\parallel v_\parallel/\omega_L)^{-1}$. Here, $k_\parallel = k_\phi B_\phi/B + k_\theta B_\theta/B$, and $k_\eta = k_\theta B_\phi/B - k_\phi B_\theta/B$ is the perpendicular component of the lower hybrid wavenumber with respect to the magnetic field projected on the magnetic surface the area of which is s(r). The lower hybrid diffusion coefficient is given by $D_{LH}=(1/2|k_{L\perp}|)(\omega_L/k_{L\perp})^2(qE_{L\perp})^2/m^2$ for $v_\perp>\omega_L/k_{L\perp}$, and $D_{LH} = 0$ elsewhere. ω_L and $k_{L\perp}=\sqrt{k_\eta^2+k_{\perp r}^2}$ are the angular frequency and perpendicular wavenumber of the LH wave, respectively. $k_{\perp r}$ is the radial component of the wave vector. $E_{L\perp}$ is the perpendicular electric field component of the LH wave. In recent works [3,12,13], the present LH operator

without the radial diffusion part and averaged over the parallel velocity has been applied for the evaluation of the LH wave damping on alpha particles and ICRF-produced minority ions. Including the parallel velocity term but neglecting the radial diffusion, the operator (2) agrees with the quasilinear model [14] derived in local velocity space for uniform configuration space in the presence of finite parallel wavenumber component. In the recent work of the LH wave interaction with alpha particles [15], it is found that the fast ion current predicted from the momentum transfer term $G_v\partial / \partial v_{||}$ is vastly dominated for localised waves by the bootstrap current generation mechanism ensuing from the terms on the left-hand side of Eq. (1). The radial diffusion term in Eq. (3) may become of importance when other diffusion mechanisms are weak, and has been recently investigated by 2D Fokker-Planck calculations [16].

In addition to the LH operator in Eq. (1), the operator for the ion cyclotron heating [17]

$$Q_{IC} = \frac{1}{v_\perp}\frac{\partial}{\partial v_\perp} v_\perp D_{IC} \left| J_{n-1}(k_{I\perp} v_\perp / \Omega) + \frac{E_{IC-}}{E_{IC+}} J_{n+1}(k_{I\perp} v_\perp / \Omega) \right|^2 \frac{\partial f}{\partial v_\perp} \qquad (4)$$

with $D_{IC} = R_{IC} q^2 |E_{IC+}|^2 / (8 m^2 n \Omega r |\sin\theta_{IC}|)$ has been incorporated. The perpendicular amplitude of the left-handed wave component, perpendicular wavenumber and the heating mode (n = 1 for fundamental harmonic heating) of the ICRF wave are denoted by E_{IC+}, $k_{I\perp}$, and n, respectively. E_{IC-} is the amplitude of the right-handed wave component. Moreover, R_{IC} is the major radius at the position where the particle crosses the cyclotron resonance layer, θ_{IC} is the poloidal angle at this point, and J_n denotes the Bessel function. In the ICRF operator, symmetrically launched fast magnetosonic waves are assumed, i.e., drift in parallel velocity and radius [18] are neglected. For simplification, also the related diffusion in $v_{||}$ and r is neglected.

With the expansion $f(t,\varphi,\theta,v_\perp,v_{||}) = f_0(v,\lambda,\varphi)+f_1(v,\lambda,\theta,\varphi)$ to first order in $\rho_L/L << 1$ and approximating $\tau_B/\tau_s << 1$, where ρ_L is the poloidal Larmor radius of the fast ions, L is the gradient scale length for the plasma and wave parameters, τ_B is the bounce time of the ion banana orbits and $\tau_s^{-1} = q^2 e^2 \ln\Lambda n_e \sqrt{2m_e/\pi} / 12\pi\varepsilon_0^2 m (k_B T_e)^{3/2}$ is the inverse slowing-down time of the ions by the electron drag, one finds the lowest-order solution from the flux-surface averaged equation

$$\left\langle \frac{\partial f_0}{\partial t} \right\rangle = \left\langle (B / v_{||}) \left[C(f_0) + Q_{LH}(f_0) + Q_{IC}(f_0) + S(f_0, v) \right] \right\rangle. \qquad (5)$$

Here $\langle ... \rangle = \oint d\theta\ (r/B_\theta)\ (...) / \oint d\theta\ (r/B_\theta)$ denotes the flux surface average. We have denoted the electron mass and charge by m_e and e, respectively, the electron temperature by T_e and the electron density by n_e. The Coulomb logarithm for the ion-electron interaction is $\ln\Lambda$, and the vacuum permittivity is ε_0. A fundamental assumption in obtaining Eq. (5), in addition to $\rho_L / L << 1$ and $\tau_B / \tau_s << 1$, is that both the slowing-down time τ_s and the characteristic LH

and ICRF diffusion times are long compared with the trapped particle bounce time. To first order in ρ_L/L, f_1 has to satisfy

$$f_1 = -\frac{m}{qB_\theta} v_\parallel \frac{\partial f_0}{\partial r}. \tag{6}$$

While the lower hybrid and ICRF wave power density absorbed by fast ions can be evaluated from the integrals $P_{LH} = \int d\vec{v}(1/2)mv^2 Q_{LH}(f_0)$ and $P_{IC} = \int d\vec{v}(1/2)mv^2 Q_{IC}(f_0)$, f_0 by symmetry does not contribute to the bootstrap current. The bootstrap current can be found with the help of the first order distribution f_1 as [19]

$$j_B \equiv q\int v_\parallel f d\vec{v} = q\frac{\pi}{h}\sum_{\sigma=\pm}\int_0^\infty\int_0^h f_1 v^3 dv d\lambda, \tag{7}$$

where the sum over σ denotes summing over both directions of the parallel velocity.

Following the method developed in Refs. [17,12,3] for description of the fast ion distribution by expanding it in Legendre polynomials in the variable $\mu = v_\parallel/v$, averaging over μ, and neglecting coupling to higher order terms and neglecting wave-induced radial diffusion, it is possible to write Eq. (5) in a form

$$\begin{aligned}\frac{\partial f_0}{\partial t} = {} & \frac{1}{v^2}\frac{\partial}{\partial v}\left[\left(-\alpha v^2 + \frac{1}{2}\frac{\partial}{\partial v}(\beta v^2)\right) f_0\right] + \frac{1}{v^2}\frac{\partial}{\partial v}\frac{\pi}{2}\frac{D_{LH}}{v} H(v - \omega_L / k_{L\perp})\frac{\partial f_0}{\partial v} \\ & + \frac{1}{v^2}\frac{\partial}{\partial v} v^2 \hat{D}_{IC}\frac{\partial f_0}{\partial v},\end{aligned} \tag{8}$$

where α and β are the Couloumb diffusion coefficients [17]. Here, H is the Heaviside function and the symmetrized ICRF diffusion operator

$$\hat{D}_{IC} = \frac{D_{IC}}{2}\int_{-1}^{1}(1-\mu^2)\left|J_{n-1}\left(\frac{k_{L\perp} v}{\Omega}\sqrt{1-\mu^2}\right) + \frac{E_{IC-}}{E_{IC+}} J_{n+1}\left(\frac{k_{L\perp} v}{\Omega}\sqrt{1-\mu^2}\right)\right|^2 d\mu \tag{9}$$

has been introduced. Eq. (8) can be solved straightforwardly for f_0 to find for steady-state

$$f_0(r,v) = f_0(r,0)\exp\left[-\int_0^v dv \frac{-\alpha v^2 + \frac{1}{2}\frac{\partial}{\partial v}(\beta v^2)}{v^2\left(\frac{\pi}{2}\frac{D_{LH}}{v^3} H(v - \omega_L / k_{L\perp}) + \hat{D}_{IC}\right) + \frac{1}{2}\beta v^2}\right] \tag{10}$$

As the ICRF heated ions become mostly trapped with $\lambda = 1 + \varepsilon\cos(\theta_{IC})$, the anisotropic effects to f_0 can be included by adopting an angle-dependent distribution function

$$f_0(r,v,\lambda) = 4\pi H(h-\lambda)H(\lambda - 1 - \varepsilon\cos\theta^*)\frac{f_0(r,v)}{\int_{-\theta^*}^{\theta^*} 2h\sqrt{1 - \frac{1+\varepsilon\cos\theta^*}{1+\varepsilon\cos\theta}}}, \tag{11}$$

where $f_0(r,v)$ is normalised as $\int_0^\infty 4\pi v^2 f_0(r,v)dv = n(r)$ with $n(r)$ denoting the minority density. Here, $\theta^* \propto \theta_{IC}$, with $\cos(\theta^*) < \cos(\theta)$, describes the maximum tip angle of the ICRF heated ions set by various orbit diffusion mechanisms. Substitution of this solution in Eqs. (6) and (7) gives an estimate of the bootstrap current of the fast ions, the goodness of which depends on the choice of θ^* and on the validity of the assumption that the v and λ dependencies in $f_0(r,v,\lambda)$ can be separated. The angle parameter θ^* in the following is determined from $\tan(\theta^*) = 2\tan(\theta_{IC})$ so that θ^* grows with θ_{IC}.

The bootstrap current after averaging over θ becomes

$$j_B = -\varepsilon \frac{m}{3B_\theta} \frac{\int_{-\theta^*}^{\theta^*} \left[(\cos\theta - \cos\theta^*)^{3/2} / h\right] d\theta}{\int_{-\theta^*}^{\theta^*} \left[(\cos\theta - \cos\theta^*)^{1/2} \sqrt{h}\right] d\theta} \int_0^\infty \frac{\partial f_0(r,v)}{\partial r} 4\pi v^4 dv. \qquad (12)$$

It should be noted that the present solution is a variant of the expression of Taguchi [5], where f_0 was described as a delta function of λ at $1 + \varepsilon\cos\theta_{IC}$. By also taking into account the untrapped particles, the described method for the calculation of the fusion alpha bootstrap current in the presence of anisotropic LH heating has been recently shown to give good results [15] for modest heating power.

In the presence of finite orbit effects by toroidicity, the expression (10) may give too peaked distributions in radius when the RF source $\frac{\pi}{2}\frac{D_{LH}}{v^3} H(v - \omega_L / k_{L\perp}) + \hat{D}_{IC}$ is calculated from the local values of the diffusion coefficients. In order to compare the present analytical model with the toroidal simulation results, we replace $\frac{\pi}{2}\frac{D_{LH}}{v^3} H(v - \omega_L / k_{L\perp}) + \hat{D}_{IC}$ by the expression $P_c(r)/[3mn(r)]$, where $P_c(r)$ is the density of collisional power transfer from the fast ions to the bulk particles obtained from the simulation. With this replacement the finite orbit broadening effects can be incorporated into the model without the need to describe the orbit trajectories analytically. The aim of the present method is to justify the use of the expressions (6), (10), and (12), where the analytical modelling of the finite orbit effects can then be performed with wanted methods.

2.2 Numerical Models

Both Monte Carlo and Fokker-Planck simulations are based on the preassumed radius dependent ICRF diffusion coefficient $D_{IC}(W_\perp, r)$ evaluated using the Gaussian spatial dependence of the electric field $|E_{IC+}(r)|^2 = |E_{IC+}|^2 \exp) - (z_{IC}^2 / L^2)$ over the plasma cross section. Here, $z_{IC}(r) = r|\sin(\theta_{IC})|$ is the vertical coordinate of the crossing point of the magnetic surface at radius r and the cyclotron resonance, and L is the electric field profile parameter. The LH wave field has been evaluated with the ray-tracing code FRTC [20] by including the wave damping on electrons. The plasma density and temperature are assumed to have radial

dependencies $n,T = (n_0,T_0 - n_{edge},T_{edge}) \times (1 - r^2/a^2)^{\alpha_{n,T}} + n_{edge},T_{edge}$, where n_0 and T_0 denote the density and temperature values on the plasma axis, a is the plasma minor radius, and $n_{edge} = 0.01 n_0$ and $T_{edge} = 0.05 T_0$.

2.2.1 2D Fokker-Planck Code

For numerical calculations of the fast ion distribution and the RF power densities absorbed by fast ions, Eq. (5) is solved with a two-dimensional Fokker-Planck code for $f_0(v_\perp,r)$. For simplicity, cylindrical geometry in configuration space with velocity distribution averaged over the parallel velocity and with the collision operator [17]

$$C(f) = -\frac{1}{v_\perp}\frac{\partial}{\partial v_\perp}(\alpha v_\perp f) + \frac{1}{2v_\perp}\frac{\partial^2}{\partial v_\perp^2}(\beta v_\perp f) + \frac{1}{4v_\perp}\frac{\partial}{\partial v_\perp}(\gamma f), \tag{13}$$

is adopted. Zero-flux boundary conditions [21] are used at small and large perpendicular velocity limits. A similar condition is also applied at the minor axis r = 0. Near the plasma edge r = a, the distribution is assumed to be Maxwellian with a fixed temperature relevant for local edge plasma conditions. Because of the cylindrical approximation, no bounce averaging is used. No isotropization of the RF operators is assumed and, consequently, the ensuing distribution function f_0 cannot be used for the calculation of the bootstrap current from Eq. (12). The ray-tracing code FRTC is used to evaluate the lower hybrid wave diffusion coefficient operator averaged over the ray ensemble and parallel refractive index as

$$\hat{D}_{LH}(r,v_\perp) = \frac{q^2e^2}{m^2\omega_L}\left\langle \int dn_{L\parallel} \frac{|E_{L\perp}(n_{L\parallel})|^2}{(1-(c/n_{L\perp}v_\perp)^2)^{1/2}}\left(\frac{c}{n_{L\perp}v_\perp}\right)^3 \right\rangle, \tag{14}$$

which is substituted for $D_{LH}/\sqrt{v_\perp^2 - \omega_L^2/k_{L\perp}^2}$ in the Fokker-Planck code. Here, c is the speed of light, and $n_{L\parallel}$ and $n_{L\perp}$ denote the refractive index components of the LH wave along and perpendicular to the magnetic field, respectively. Also, in the coefficient of G_r the average value of k_η from the ray tracing spectrum is applied and $v_\parallel = G_v = 0$ are assumed.

As an initial condition, a Maxwellian thermal minority velocity distribution with a radial density and temperature profile of the background plasma is adopted. To obtain stationary conditions, an operator for the anomalous radial diffusion of the fast ions by mechanisms different from those caused by the wave is added with a form

$$S(f) = \frac{1}{r}\frac{\partial}{\partial r} r D_{an}\left(1 - \frac{r^2}{a^2}\right)\frac{\partial f}{\partial r} + \frac{1}{r}\frac{\partial}{\partial r}\frac{2r^2\alpha_n D_{an}}{a^2} f. \tag{15}$$

This operator, with the diffusion coefficient D_{an} modelled phenomenologically, guarantees the recycling of the centrally heated minorities and thermal minority ions produced

near the plasma edge and makes it possible to obtain stationary conditions in the presence of wave-induced diffusion mechanisms [16]. It also maintains the parabolic radial density distribution. Experimentally, the ion radial diffusion coefficient has been observed to have a few times the neoclassical value, and is usually explained in terms of either magnetic ripple, stochasticity, or MHD modes.

2.2.2 Monte Carlo Code

For fully toroidal calculations, guiding centre equations of motion for the fast ions in the toroidal magnetic configuration are solved with the Monte Carlo code ASCOT [8,22] in the presence of Monte Carlo operators corresponding to the RF and collision models in Eqs. (1-4). These calculations cover the self-consistent effects of a minority ion distribution in velocity and configuration space, the finite orbits, radial neoclassical diffusion and current generation in a tokamak magnetic configuration. The code calculates diffusion, power deposition, and energy exchange of the fast particles with the waves, and contains the operators for collisional slowing-down, pitch angle scattering, and energy diffusion of particles, in combination with operators for the wave interaction and for any anomalous radial diffusion, assuming a thermal source of minority ions from the plasma edge to obtain stationary conditions. The guiding-centre orbits of the particles are tracked in a tokamak geometry with elongation, D-shape and Grad-Shafranov displacement of magnetic axis.

Based on the results of Ref. [8] for the fast ion LH wave interaction, the Monte Carlo operators

$$\Delta W_\perp = (1/s)[\partial/\partial W_\perp - (k_\eta / m\omega\Omega)\beta(\partial/\partial\rho)](s\hat{D}_{LH})\Delta t \pm \sqrt{2\hat{D}_{LH}\Delta t}, \qquad (16)$$

$$\Delta\rho = -\Delta W_\perp (k_\eta / m\omega_L\Omega)\beta, \qquad (17)$$

$$\Delta p_\phi = (k_\phi R/\omega)\beta\Delta W_\perp, \qquad (18)$$

are adopted for the changes of the particle perpendicular energy $W_\perp$, the magnetic surface coordinate $\rho = r$, and the toroidal momentum p_φ by the LH wave during the time step Δt. The LH diffusion coefficient $\hat{D}_{LH}$ is given here as $(1/2|k_{L\perp})(\omega_L / k_{L\perp})^2 (qE_{L\perp})^2 / \sqrt{v_\perp^2 - \omega_L^2 / k_{L\perp}^2}$.

The operators for Δp_ϕ and $\Delta\rho$ are directly proportional to $\Delta W_\perp$, and have been added for investigations of interaction for the asymmetric launching or for the poloidal propagation of the LH wave. It should be noticed that with $k_\eta = 0$ and $k_\phi = 0$ the operator system in Eqs. (16-18) becomes equivalent with the operator in Eq. (2) in the absence of diffusion in parallel velocity and radius. In writing Eq. (16), $\hat{D}_{LH}$ has been assumed not to depend on $v_\parallel$, which similarly to the other assumptions is valid if $W_L >> \Omega$, $|k_\chi v_\parallel|/\omega_L << 1$, and $|\Delta v_\parallel| << |\Delta v_\perp|$. The time

step in the operators has to be chosen small enough so that $\sqrt{2\hat{D}_{LH}\Delta t}\,/\,W_{\perp} << 1$ in order to ensure sufficiently accurate statistics.

For the change of the perpendicular velocity according to the operator (4), the Monte Carlo operator presented in Ref. [23]

$$\Delta v_{\perp} = \frac{q}{2m} T e^{-z/L} e^{i\delta} [E_{IC+} J_{n-1}(\frac{k_{I\perp} v_{\perp}}{\Omega}) + E_{IC-} J_{n-1}(\frac{k_{I\perp} v_{\perp}}{\Omega})], \qquad (19)$$

is applied. Here, z is the coordinate vertically along the cyclotron resonance from the median plane, and the phase angle δ is a uniformly distributed random number between 0 and 2π. The change in $v_{\perp}$ by the operator in Eq. (19) is calculated only when the ion passes through the ion cyclotron resonance. This incremental change is proportional to the resonance duration time τ calculated in Ref. [23] for different orbit topologies. The diffusion in parallel velocity and radius [18] by the ICRF wave are neglected.

In the calculations, the initial coordinates of the particles are evenly distributed in the poloidal cross section of an axisymmetric plasma in proportion to the initial local minority density. The particles are evenly distributed in the pitch $v_{\|}/v$ with a total velocity equal to the background thermal velocity, and they are followed until they escape the plasma, or a time limit has been achieved. By recording the energy exchange with the waves and the time integral of the particle parallel velocity at each radius and time instant, the steady-state current profile, the power deposition/absorption profiles, and the total energy given or extracted by the waves can be obtained. Because the particle motion in radius is restricted by the natural constraints at $\rho = 0$ and $\rho = a$, no particular conditions are applied in configuration space.

3. RESULTS

3.1 Interaction of LH Waves with Minority Ions

The interaction of the LH and ICRF waves with the hydrogen minority ions is studied with the Fokker-Planck calculations for two JET configurations: JET I and JET II, described in Table 1. Firstly, the case where the LH wave is unable to penetrate to the inner parts of the plasma due to high electron temperature and density is considered. As a second case, strongly penetrating LH waves are considered with parameter values similar to a low density, low temperature JET discharge. To elucidate the significance of spatial overlap of the LH and ICRF waves, two different locations of the resonant region of the ICRF wave are considered and the calculations are done both in the absence and presence of anomalous radial diffusion.

3.1.1 Weakly Penetrating LH Wave

In the first case (JET I, see Table 1), a hydrogen minority in a deuterium-tritium (DT) plasma with a high background temperature of $T_{i,e}$ = 10 keV is considered. Flat density and temperature profiles with $\alpha_n = \alpha_T = 0.5$ are adopted. The width L = 0.25 m is assumed for the ICRF wave interaction, and the right-hand component of the wave is neclected i.e. $|E_{IC-}| = 0$. From the ray tracing, the total LH wave power absorbed by electrons is P_{LH} = 4.8 MW. The LH wave diffusion coefficient $\hat{D}(r, v_\perp)$ obtained from ray-tracing is shown in Fig. 1. As the diffusion coefficient is small with $v_\perp < 1.5 \times 10^7$ m/s at radii less than 0.5a, the ICRF tail ions interact there weakly with the LH wave.

In figures 2a and 2b, respectively, the LH and ICRF power absorbed by the minority ions is depicted. In the ray-tracing the real JET geometrical configuration with the ellipticity 1.68 and triangularity 0.1 are used, while the Fokker-Planck calculations are done in the cylindrical geometry with a = 1.1 m. Consequently, the total power absorptions are obtained by multiplying those shown in Figures 2a and b by a factor 1.68. Initially the LH power absorption is zero because there are very few particles in the LH region in velocity space. On the other hand, the power absorption from the ICRF wave has its maximum, because there is a lot of ions in the thermal region to be heated. In Figure 2b, we can notice that the ICRF power absorption decreases fast and reaches the steady-state when the high-energetic tail is formed. In case with an off-axis localised ICRF wave, the power absorbed from the LH wave increases rapidly during the rail-formation when more and more ions reach the velocity range of the LH absorption. When the centre of the ICRF wave is on the plasma axis, LH wave absorption remains small or negligible because the LH wave is not present in the region where the ICRF heated ions are. However, in the presence of radial diffusion, some of the heated particles are diffused to the outer radius and modest LH absorption can be observed. Anomalous radial diffusion also increases the ICRF power absorption because thermal ions from the plasma boundary are diffused to the ICRF region to be heated.

In Figures 2c and d, the time-average over two seconds of the LH and ICRF deposition profiles, respectively, are presented. In the case with a wide overlap and zero radial diffusion, the shapes of the LH and ICRF power deposition profiles are similar, because the number of particles reaching the LH interaction range in energy depends on the ICRF power absorption at the same spatial location. When anomalous radial diffusion is present, wider LH power deposition profile is obtained which extends to plasma boundary where it vanishes because the thermal Maxwellian distribution is used as a boundary condition.

Figure 3 shows the corresponding result to Figure 2 for the ICRF and LH power deposition from the fully toroidal Monte Carlo simulation in the absence of anomalous radial diffusion. Off-axis cyclotron resonance at r = 0.4 m is assumed. Finite orbit effects are found to

broaden the deposition profiles somewhat but the total absorption levels of the cylindrical calculation are well reproduced from the toroidal simulation.

3.1.2 Strongly Penetrating LH Wave

For the case with low density and low temperature, parameters similar to the JET discharge 33153 are used (JET II in Table 1). Hydrogen minority in deuterium plasma with carbon and beryllium impurities is considered with a profile constant $\alpha_n = 0.25$. Temperatures for electrons and background ions on the axis are $T_e(0) = 5.88$ keV and $T_i(0) = 2.68$ keV, respectively, with the profile constant $\alpha_T = 1.5$. The LH wave absorption on electrons from the ray-tracing is $P_{LH} = 4.8$ MW.

When the ICRF wave is centred on the axis, the interaction width L = 0.4 m is used to obtain the ICRF power absorption of 5.1 MW. As in previous section, calculations are done also for an off-axis localised ICRF wave with the centre and profile width $r_{IC} = 0.4$ m and L = 0.25 m, respectively. Fixed value $E_{IC}/E_{IC+} = 4$ with $|E_{IC+}| = 3$ kV/m is used for the relation between right and left-hand circularly polarised wave components.

In Figure 4a, the LH power absorbed by the minority ions is depicted. Finite absorption is observed in all cases because the LH wave is now able to penetrate deeper into the plasma due to lower density and temperature. It should be noted that as previously the total power absorptions in Figures 4a and 4b have been scaled up by a factor of 1.68 to obtain the total absorption levels. In Figure 4b, the ICRF power absorption is represented. Unlike in previous section (see Figure 2b) where the time evolution of the ICRF power absorption level was monotonic, the initial transient is now more complicated. Increase in power absorption after the initial drop is assumed to take place because of the strong contribution of the right hand component of the wave. In Figure 4c and d, the LH and ICRF power deposition profiles are depicted, respectively. The LH wave absorption is observed to take place also near the centre.

In the previous examples, the perpendicular LH wave vector component is assumed to be radially directed. Consequently, the wave-induced diffusion due to nonradial wavenumber components is neglected. Including a finite poloidal wavenumber $k_\eta = 3000$ m^{-1} in the example of strong LH penetration, the LH wave absorption was found to be negative, i.e. the energy of ICRF heated minority ions was transferred to the LH wave, if the LH wave-induced radial drift was outwards for the ions giving energy to the wave. This extraordinary result is of a great similarity to the prediction of Fisch and Rax [7] for special fusion alpha particle ensembles interacting with the localised LH wave and was obtained from the cylindrical calculation with strongly centred ICRF power deposition and with well overlapping LH interaction regime. Here, the rapidly decreasing LH wave-ion velocity interaction regime for increasing radius and the high anisotropy of the ICRF heated ions, as well as the reflecting boundary for the ion diffusion on the axis, play an important role in reversing the direction of power transfer

between the ions and the LH wave. Unfortunately, in full toroidal Monte Carlo calculations, where the large orbit widths of the fast ions make the ions relatively insensitive to the details of the LH wave structure, positive absorption was observed for both inward and outward directed LH wave-induced radial diffusion. Nevertheless, the present result of wave amplification by fast ions for very special conditions in cylindrical approximation may guide to construct the proper environment for this purpose in the toroidal geometry. It is worth noticing that in the presence of strong ICRF heating, most ions are trapped and the radial coordinate of the tip of the trapped ion bananas would be unaffected by the nonradial perpendicular wave propagation. However, in toroidal geometry, the wave-induced radial diffusion becomes relevant for the trapped ions by means of finite toroidal momentum transfer.

3.2 RF-Generated Bootstrap Current

In order to see the effects of the RF waves on the fast ion currents, toroidal simulations are performed. In Figure 3a, the fast ion current density is shown for the case of weak LH penetration of the previous Section. Around the cyclotron resonance at r = 0.4 m, a bipolar modification of the current density is found. This current is observed both in the presence and absence of the LH wave. Together with the Monte Carlo results, the analytical result from the estimates Eqs. (12) and (10) is shown which relatively well reproduces the fast ion current profile from the simulations. The lower hybrid waves are found to enhance the current, but their effect remains relatively small because of the small LH absorption in the present case.

In Figure 5a, the current density obtained from the Monte Carlo simulation and from the analytical model of Section 2 are obtained for a JET configuration (JET III in Table 1) where a high temperature $T_{i,e}$ = 10 keV and high density $n_e = 0.84 \times 10^{20}$ m^{-3} with flat profile constants $\alpha_n = \alpha_T = 0.5$ are assumed. A circular cross section with a parabolic current profile and equal deuterium and tritium concentrations with a hydrogen minority concentration of $n_H = 2 \times 10^{18}$ m^{-3} are assumed. The ICRF parameters are $|E_{IC+}| = 3$ kV / m, $k_{\perp\perp} = 30$ m^{-1}, $r_{IC} = 0.4$m, and L = 0.4 m. No LH wave is present. Here, it can be seen that the analytical model predicts well the current density levels and the formation of the bipolar current density profile. The current density of the fast ions remains below 100 kA/m^2 outside the wave regime. On the other hand, around the ICRF wave regime, significantly enhanced current density levels are obtained. In agreement with the analytical bootstrap current model, the current density is reduced inwards from the cyclotron resonance while it is increased outwards from it. The bipolar current density modification by the ICRF wave is a clear consequence of the RF heating of the minority ions and of the corresponding local increase of the average energy of the ions in this region. Figure 5b shows the ICRF wave power absorption profile. The slight underestimation of the current by the analytical model both in Figure 3a and Figure 5a follows from the bootstrap current of the thermal ions which is not included in the analytical theory.

In the present JET example, the total absolute current $\int |j_B| 2\pi r dr$ is 190 kA. The total ICRF wave power absorbed is 15.4 MW. It is worth noticing that the cyclotron resonance position in the present case was chosen on the outboard side. For the inboard resonance position at r = 0.4 m, approximately two times larger current modification was observed with the same ICRF power absorption. It is also important to note that in the present simulation, symmetric launching of the ICRF power is assumed. This means that the current generation by the momentum transfer in toroidal direction, which for the present parameters with asymmetric launching for toroidal wavenumber of 10 m^{-1} would give a comparable contribution in addition to the bootstrap mechanism, is overlooked. However, it is of great importance to note that the current density can be also modified by symmetric launching.

Figure 6a shows the current density profile for the ions for the ITER-sized parameters (ITER in Table 1) as obtained from the Monte Carlo simulations and from the analytical estimate, Eqs. (12) and (10). The results are calculated for the ICRF wave parameters $E_{IC} = 2500V / m, k_{I\perp} = 30m^{-1}, r_{ci} = -1.6m$, and $L = 1.5m$. Here, the cyclotron resonance of the hydrogen minority lies on the high field side inboard from the axis. The LH wave frequency is f_L = 3.7 GHz, and its penetration is obtained from ray-tracing. The LH wave diffusion coefficient is roughly centred at ρ_0 = 2.4 m with the width 0.4 m. The LH wave absorption on electrons is 100 MW, and the perpendicular wave vector is found to be essentially in the radial direction and with launched toroidal refractive index spectrum between 1.2 and 2. In the simulation, 4600 hydrogen test ions are traced for two seconds with the initial hydrogen density of $n_H = 2 \times 10^{18}$ m^{-3} assumed at the plasma centre. The wave power densities shown in Figure 6b are obtained as averages over the simulation time. The anomalous diffusion coefficient D_{an} is taken to be zero in the simulations.

A fairly good agreement between the analytical result and the simulation result for the current density is found in the off-axis region around the ICRF wave regime. The current density levels obtained from the simulation are similar to those in the JET case. This is expected as the power source density and the hydrogen density are similar. In the present case, the ICRF power absorption is 35 MW and the total absolute current of the fast ions is 602 kA. Again, roughly two times smaller absolute currents were found for the outboard position of the resonance. On the other hand, the current enhancement by the asymmetric toroidal launching of the ICRF wave with the toroidal wavenumber of 5 m^{-1} was found to be relatively weak with respect to the bootstrap effect. The LH wave is found to interact weakly with the ions because of its relatively poor penetration for the present case with no enhanced radial diffusion of the fast ions. For the case when the cyclotron resonance position is nearer the centre at r = 0.4 m, an enhanced negative current density close to the axis is found from the simulation which cannot be obtained from the analytical model. The current density changes from negative values to positive ones about r = 0.5 m, and the simulation result approaches the analytical result for

the larger radii. The negative current density near the axis has been obtained in Ref. [6], and is explained by the finite orbit effects which are not included in our analytical model.

4. DISCUSSION

In 2D Fokker-Planck calculations, power deposition profiles and absorption dynamics of the LH and ICRF waves and the effects of the radial transport due to anomalous effects on their relative absorption levels were studied. Both LH and ICRF power absorption were observed to increase due to anomalous diffusion, because of the ICRF heated ions diffusing from the centre to the LH region and thermal ions diffusing from the plasma edge to the ICRF region. For the chosen JET configurations, the LH wave absorption on ICRF heated minority ions was found to be only about 10% of the both ICRF and LH heating power. The relatively low LH absorption agrees well with the prediction obtained by de Andrade *et al.* [3] with simplified methods. However, it should be noted that for well overlapping localised LH and ICRF interaction regimes, significantly larger absorption can be predicted.

The analytical model derived in Section 2 explains satisfactorily the bipolar fast ion minority current density profile and its main parameter dependences obtained from the toroidal simulations in the presence of ion cyclotron resonance and Landau absorption mechanisms for the ICRF produced fast ion interaction for a JET-sized and reactor-sized tokamak. The model obtained from the first order expansion of the drift Fokker-Planck equation to the Larmor parameter within a small bounce period limit has been derived in the weak RF wave and small ε approximation by neglecting the pitch angle scattering effects. Because the major effect for the bootstrap current enhancement is found to arise from the ion heating in the presence of finite critical velocity v_c for the slowing-down, the inclusion of pitch angle scattering (important for $v \leq v_c$) could be considered as significant. We note also that the bootstrap current calculated in the present paper should be corrected by the factor $[1 - (Z_i/Z_{eff}) (1 - 1.46\varepsilon^{1/2})]$ in order to account for the back electron current opposing the ion current. Here, Z_i is the ion charge number, and Z_{eff} is the effective charge number of the plasma. This factor may vary between, say, 0.25 and 0.75 around the mid-radius of a reactor.

The appearance of a bipolar bootstrap current density profile by the localised ICRF or LH wave interaction with current density levels far exceeding the thermal bootstrap current density and wave driven ion current density by momentum transfer suggests and improvement in the efficiency of the wave generated ion current. It is of great importance to note that the bootstrap current can be generated also with the symmetric launching. Although the net current is also increased by the bootstrap current enhancement, the particular form of the current density profile appears more beneficial for the evident shear production for stabilisation of plasma instabilities. It should be noted that in any reversed magnetic shear equilibrium [24], where the

necessary current profile is relatively flat, only a small amount of auxiliary perturbation in the current density may need to be added to shape the current profile properly.

In the calculations, the LH wave propagation was obtained from ray-tracing but the ICRF wave diffusion operator has been assumed fixed with Gaussian profiles. The inclusion of realistic operator forms based on a spectrum of waves obtained by wave codes with full absorption models (including both electron and ion damping) is important but is beyond the present paper and is left for future work.

ACKNOWLEDGEMENTS

This work was supported by the Finnish Ministry of Trade and Industry and the Academy of Finland.

REFERENCES

[1] Wong K-L Ono M 1984 *Nucl. Fusion* **24** 615

[2] Lam NT *et al* 1994 *Nucl. Fusion* **34** 1116

[3] Ramos de Andrade MC *et al* 1994 *Plasma Phys. Contr. Fusion* **36** 1171

[4] Hellsten T *et al* 1995 *Phys. Rev. Lett.* **74** 3612

[5] Taguchi M in Controlled Fusion and Plasma Physics (Proc. 21th Eur. Conf. Montpellier, 1994) Vo. 18B Part III European Physical Society (1994) 1142; Chang C S 1995 Phys. Plasmas **2** 3696

[6] Core W G F and Cottrell G A 1992 *Nucl. Fusion* **32** 1637

[7] Fisch N J and Rax J-M 1992 *Phys. Rev. Lett.* **69** 612

[8] Heikkinen J A and Sipilä S K 1995 *Physics of Plasmas* **2** 3724; Heikkinen J A and Sipilä S K 1995 *Phys. Rev. E* **51** 1655

[9] Pavlo P, Krlín L and Tluchor 1991 *Nucl. Fusion* **31** 711

[10] Rosenbluth M N *et al* 1972 *Phys. Fluids* **15** 116

[11] Karney C F F 1979 *Phys. Fluids* **22** 2188

[12] Barbato E and Santini F 1991 *Nucl. Fusion* **31** 673

[13] Fisch N J and Rax J-M 1992 *Nucl. Fusion* **32** 549

[14] Anderson D *et al* 1991 *Phys. Fluids B* 3 3125

[15] Heikkinen, J A and Sipilä S K , "Alpha Current Driven by Lower Hybrid Heating of Thermonuclear Alpha Particles in Tokamak Fusion Reactors", to appear in Nuclear Fusion.

[16] Heikkinen J A and Kiviniemi T P, "Ion Cyclotron Minority Ion Heating in the Presence of Lower Hybrid Waves", to appear in Physics Letters A.

[17] Stix T H 1975 *Nucl. Fusion* **15** 737

[18] Chen L *et al* 1988 *Nucl. Fusion* **28** 389

[19] Hsu C T, Catto P J and Sigmar D J 1990 *Phys. Fluids B* **2** 280; Hsu C T , Shaing K C Gormley R P and Sigmar D J 1992 *Phys. Fluids B* **4** 4023; Taguchi M 1992 *J. Phys. Soc. Japan* **61** 4443

[20] Saveliev A and Piliya A 1995, submitted for publication in Nuclear Fusion.

[21] Morishita T *et al* 1987 *Nucl. Fusion* **27** 1291

[22] Heikkinen J A *et al* 1993 *J Comp. Phys. Commun.* **76** 215

[23] Kovanen M and Core W G F 1993 *J. Comput. Phys.* **105** 14

[24] Kessel C, Manickam J, Rewoldt G and Tang W M 1994 *Phys. Rev. Lett.* **72** 1212

Table 1: Simulation parameters forJET and ITER configurations

	JET 1	**JET II**	**JET III**	**ITER**
a [m]	1.1	0.89	1.1	2.8
R [m]	2.95	2.95	2.95	7.75
B_t [T]	3.4	3.4	3.4	6.2
I_p [MA]	3	3	3	15
n_e [10^{20} m^{-3}]	0.4	0.296	0.84	0.84
n_D [10^{20} m^{-3}]	0.19	0.0728	0.41	0.41
n_T [10^{20} m^{-3}]	0.19	0	0.41	0.41
n_H [10^{18} m^{-3}]	2	0.364	2	2
n_{Be} [10^{18} m^{-3}]	0	2.19	0	0
n_C [10^{18} m^{-3}]	0	2.19	0	0
T_e [keV]	10	5.88	10	20
T_i [keV]	10	2.68	10	20
α_n	0.5	0.25	0.5	0.5
α_T	0.5	1.5	0.5	0.5
$E_{IC+}\left[\frac{kV}{m}\right]$	3	3	3	2.5
$E_{IC-}\left[\frac{kV}{m}\right]$	0	12	12	0
r_{IC} [m]	0/0.4	0/0.4	0.4	-1.6
L [m]	0.25	0.4/0.25	0.4	1.5
$k_{I\perp}$ [m^{-1}]	30	29	30	30
f_L [GHz]	3.7	3.7	3.7	3.7

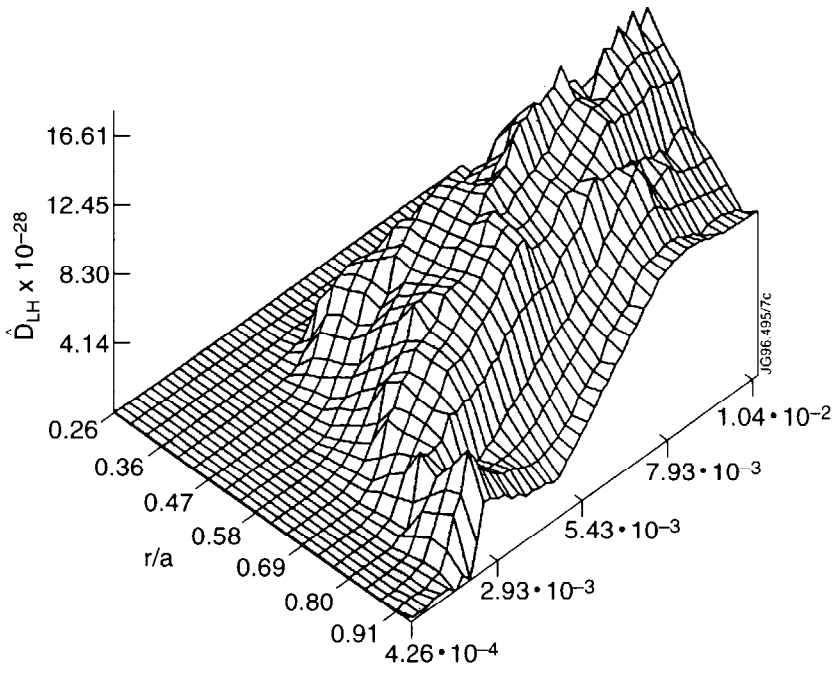

Fig.1: LH diffusion coefficient $\hat{D}_{LH}(r, v_\perp)$ *as a function of r/a and* $(v_\perp/c)^2$ *for the JET configuration (JET I, see Table 1) with weak LH penetration obtained from ray-tracing.*

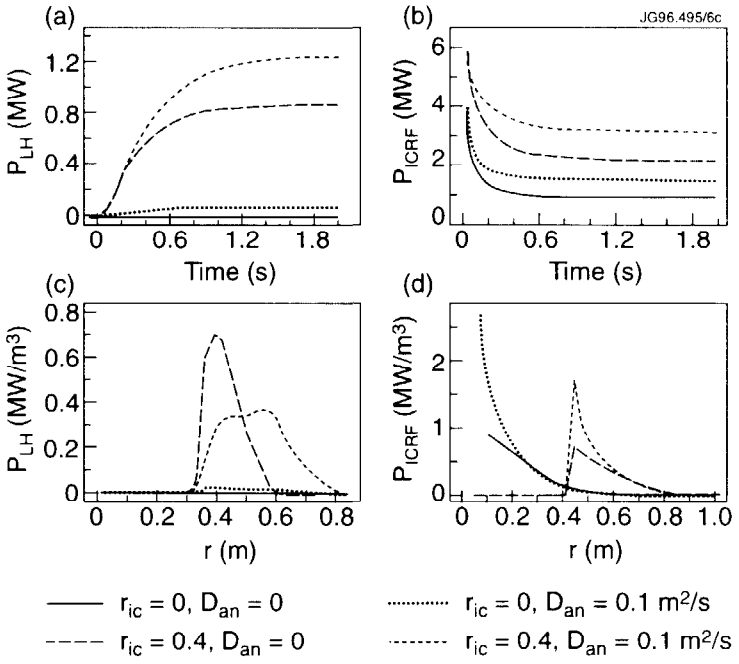

Fig.2: (a) LH and (b) ICRF power absorption as a function of time, (c) LH and (d) ICRF power deposition profiles (time average over two seconds) in the JET configuration (JET I, see Table 1) with weak LH wave penetration for various values of D_{an} *and* r_{IC}.

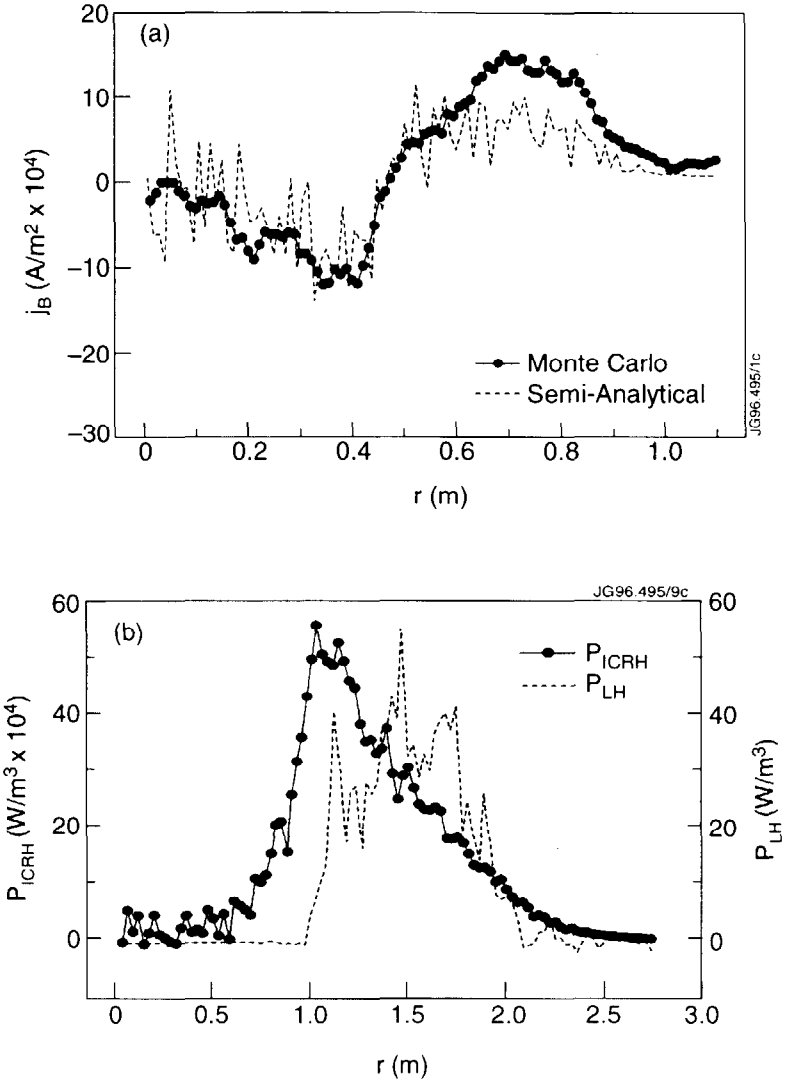

Fig.3: (a) Current density profile for the JET configuration (JET I, see Table 1) with weak LH wave penetration from toroidal Monte Carlo simulation and from the analytical mode. (b) ICRF and LH power deposition profiles. $D_{an} = 0$ *and* $r_{IC} = 0.4$ *m.*

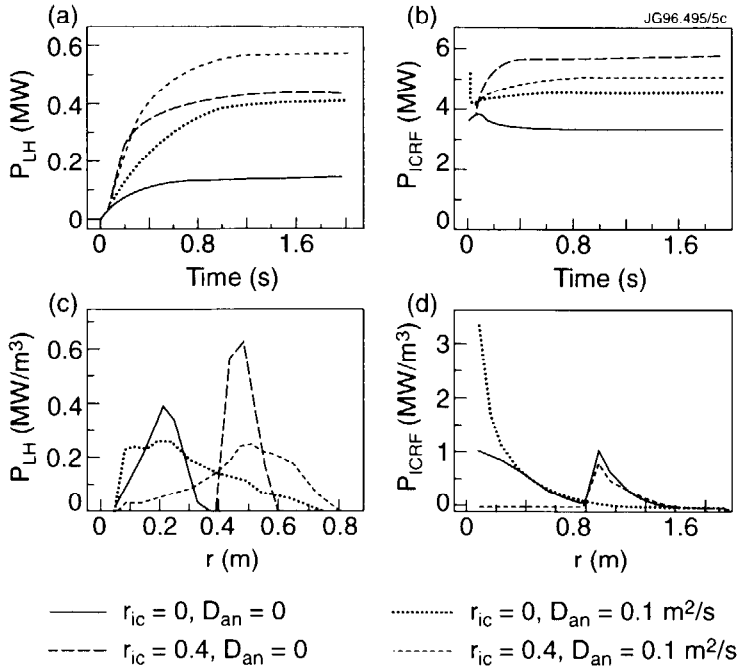

Fig.4: (a) LH and (b) ICRF power absorption as a function of time, (c) LH and (d) ICRF power deposition profiles (time average over two seconds) in the JET configuration (JET II, see Table 1) with strong LH wave penetration for various values of D_{an} and r_{IC}.

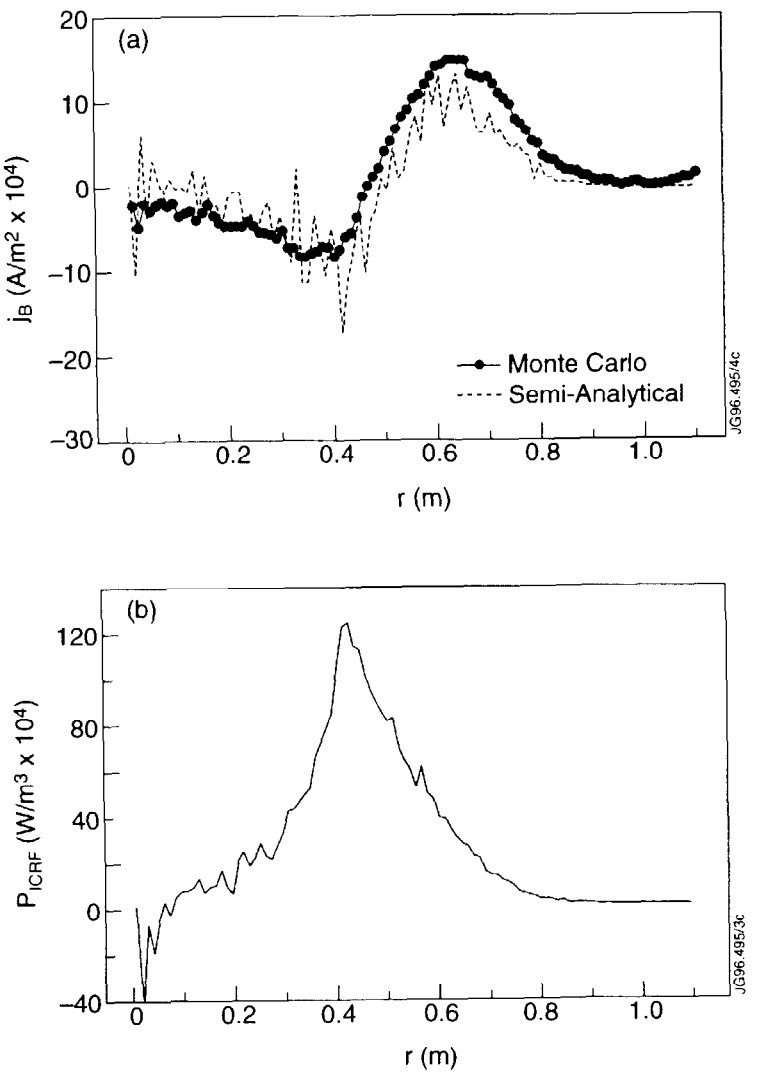

Fig.5: (a) Current density profile for the JET configuration (JET III, see Table 1) with ICRF only heating from toroidal Monte Carlo simulation and from the analytical model. (b) ICRF power deposition profile. $D_{an} = 0$ *and* $r_{IC} = 0.4$ *m.*

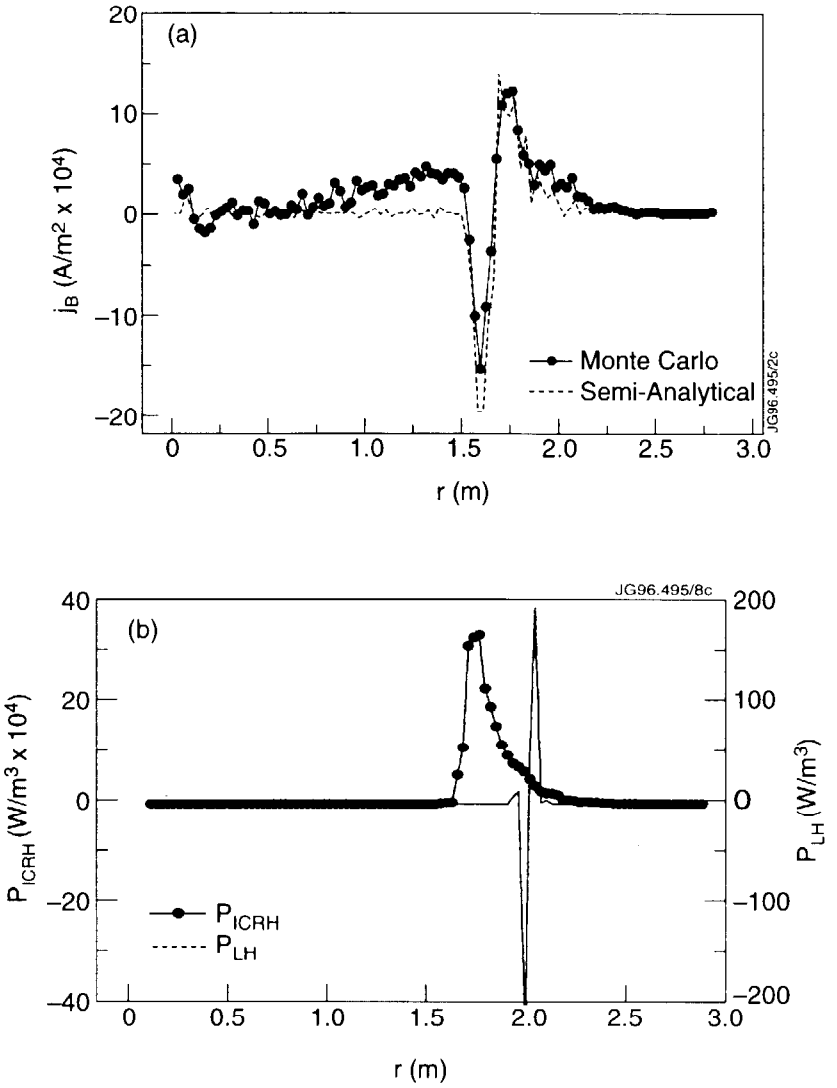

Fig.6: (a) Current density profile for the ITER configuration (ITER, see Table 1) with ICRF and LH heating from toroidal Monte Carlo simulation and from the analytical model. (b) ICRF and LH power deposition profiles. $D_{an} = 0$ *and* $r_{IC} = -1.6$ *m.*